

# Similarity for downscaled kinetic simulations of electrostatic plasmas: reconciling the large system size with small Debye length

Yanzeng Zhang,<sup>1</sup> Haotian Mao,<sup>2,1</sup> Yuzhi Li,<sup>1</sup> and Xian-Zhu Tang<sup>1</sup>

<sup>1)</sup>*Los Alamos National Laboratory, Los Alamos, NM 87545, USA*

<sup>2)</sup>*University of California at San Diego, La Jolla, California 92093, USA*

A simple similarity has been proposed for kinetic (e.g., particle-in-cell) simulations of plasma transport that can effectively address the longstanding challenge of reconciling the tiny Debye length with the vast system size. This applies to both transport in unmagnetized plasma and parallel transport in magnetized plasmas, where the characteristic length scales are given by the Debye length, collisional mean free paths, and the system or gradient lengths. The controlled scaled variables are the configuration space,  $\mathbf{x}/\mathcal{L}$ , and artificial collisional rates,  $\mathcal{L}\mu$ , which is realized through scaling the Coulomb Logarithm in the simulations,  $\mathcal{L}\ln\Lambda$ . Whereas, the scaled time,  $t/\mathcal{L}$ , and electric field,  $\mathcal{L}\mathbf{E}$ , are automatic outcomes. The similarity properties are examined, demonstrating that the macroscopic transport physics is preserved through a similarity transformation while keeping the microscopic physics at its original scale of Debye length. To showcase the utility of this approach, two examples of 1D plasma transport problems were simulated using the VPIC code: the plasma thermal quench in tokamaks [J. Li, et al., Nuclear Fusion **63**, 066030 (2023)] and the plasma sheath in the high-recycling regime [Y. Li, et al., Physics of Plasmas **30**, 063505 (2023)].

First-principles kinetic plasma simulations, with either the Particle-In-Cell (PIC)<sup>1–3</sup> or the continuum<sup>4–6</sup> approach, can provide critical insights into complex plasma dynamics, and have served as a cornerstone of high-fidelity plasma modelings. They are particularly in demand for nearly collisionless plasmas, where the plasma mean free path,  $\lambda_{mfp} \propto T_e^2/n_e$ , is much longer than the characteristic system size,  $L$ , as a result of the high plasma temperatures ( $T_e$ ), low plasma densities ( $n_e$ ), or a combination of the two<sup>7–11</sup>. Even in the opposite limit of collisional plasmas with  $\lambda_{mfp} \ll L$ , kinetic effects can still play an important role, especially when the electron distribution function deviates significantly from a local Maxwellian. These include the plasmas in the sheath and presheath regions, where the electron distribution has a one-sided cutoff in parallel velocity with respect to the magnetic field due to the electrostatic trapping effect of the sheath/presheath electric field that reflects thermal electrons for ambipolarity<sup>12,13</sup>. An even more dramatic situation of spatially-extended non-Maxwellian distribution functions arises when a nearly collisionless plasma interacts with a cold, dense, and often collisional plasma, e.g., in the plasma thermal quench (TQ) of a major disruption in tokamaks<sup>14–16</sup> and the formation of structures in a galaxy clusters<sup>17,18</sup>.

It is often the case that these high-fidelity kinetic simulations can incur extreme computational costs. The difficulty comes about because the kinetic simulation has to reconcile a large system size,  $L$ , with the small plasma Debye length,  $\lambda_D$ . This would be a physics fidelity requirement in physical systems where a localized non-neutral plasma structure is present in an otherwise quasi-neutral plasma. Such non-neutral plasma structures would have a width on the order of the Debye length due to the plasma shielding effect<sup>19</sup>. Well-known examples include the sheath in a plasma intercepting a solid<sup>20–23</sup> and the parallel collisionless shocks<sup>14,24–28</sup>, in which the shock front widths are of a few Debye lengths.

Even in a plasma without isolated non-neutral regions, the PIC or kinetic simulations in general, have to resolve the Debye length to suppress the inherent numerical instabilities when an explicit time advancing scheme is deployed<sup>1,2</sup>. In a

fusion grade plasma with temperature  $T_e \sim 10\text{keV}$  and density  $n_e \sim 10^{20}\text{m}^{-3}$ , the Debye length is orders of magnitude smaller as  $\lambda_D/L \sim 10^{-6}$ . Resolving the Debye length would bring a substantial computational cost. This is especially so in a plasma with strong density variation, for example, in a plasma TQ where the cold/dense edge plasma region has a far smaller Debye length than the initial fusion-grade core plasmas.<sup>16</sup>

One way to circumvent this obstacle is to perform downscaled PIC simulations to decipher the physics scaling laws, in which the characterized physical lengths including  $\lambda_{mfp}$  and  $L$  are proportionally reduced compared to the Debye length<sup>16,29,30</sup>. This is to some extent equivalent to artificially enlarging the Debye length through the permittivity  $\epsilon_0$  in the Poisson equation while keep the other lengths unchanged<sup>31</sup>. A more aggressive but related aim for downscaled simulations, which also applies to experimental designs, is the concept of similarity. For example, the so-called “perfect” hydrodynamic similarity has been argued by Ryutov and Remington<sup>32</sup> for simulating astrophysical phenomena on laboratory laser facilities like the National Ignition Facility. Recent works on similarity and scaling laws in the context of low-temperature plasma discharges can be found in Refs. 33–36 and in the review paper Ref. 37.

The current paper provides an analysis of our previous downscaled kinetic simulation approach from the perspective of similarity. We will show that a simple similarity exists that provides a straightforward scaling for the quasi-neutral plasmas but preserves the non-neutral plasma structures. This appears to be a “perfect” solution in electrostatic plasma simulations to reconcile the system size with the Debye length, while preserving the transport physics. Specifically, under our scaling, the plasma distribution function remains invariant almost everywhere, namely the quasi-neutral region away from the isolated spots of non-neutral plasmas. As a result, the density, velocity, pressure, and most importantly, thermal conduction heat flux of plasmas (and neutrals if present) are not scaled. In the fluid descriptions of plasmas, this means that no approximation with regard to the equation of state is needed for the

similarity<sup>32</sup>.

Our downscaled simulation approach is different from those in conventional similarity and scaling laws designed for experiments (see Refs. 32, 37–41 and references therein), in that the rates of collisions will be scaled through an *artificially* enhanced Coulomb Logarithm,  $\ln\Lambda$ , in the collisional operators. Rescaling the collision rates only through the Coulomb algorithm allows the treatment of a wide range of collisional processes including the three-body collisions in plasma-neutral interactions. Without losing generality, let's consider the electron Boltzmann equation in a partially ionized plasma in the electrostatic limit without a background magnetic field  $\mathbf{B}_0$  (the presence of  $\mathbf{B}_0$  and the electromagnetic effect are discussed in the supplemental material), which applies to the transport in multi-dimensional unmagnetized plasmas and the parallel transport in magnetized plasmas,

$$\frac{\partial f_e}{\partial t} + \mathbf{v} \cdot \frac{\partial f_e}{\partial \mathbf{x}} + \frac{q_e}{m_e} \mathbf{E} \cdot \frac{\partial f_e}{\partial \mathbf{v}} = \sum_j C_{ej}(f_e, f_j, \mathbf{v}_{ej}, \sigma_{ej}), \quad (1)$$

where  $f_e(\mathbf{x}, \mathbf{v}, t)$  is the electron distribution and  $\mathbf{E}$  is the electric field. Here  $C_{ej}$  describes the collisions between electrons and species  $j$  (including neutrals) with all the collisional types. It depends on the distributions  $f_e$  and  $f_j$ , the relative velocity  $\mathbf{v}_{ej}$ , and the cross-section of the process  $\sigma_{ej}$ . Similar Boltzmann equations can be obtained for other species' distribution functions  $f_j$ .

One interesting and important property of the collisional operators  $C_{ej}$  is that they are proportional to the collisional rates<sup>42</sup> defined as  $\mu_{ej} n_e = \int_0^\infty \sigma_{ej}(v) v_{ej} f_e(\mathbf{v}) d\mathbf{v} \propto \ln\Lambda$ . Such rates appear naturally since the collisional terms on the right-hand-side (RHS) of the Boltzmann equation represent the rates of the change of distribution function,  $\delta f_e / \delta t$ , in a given region of phase space as a result of collisions.

Under the transformation of

$$t \rightarrow t/\mathcal{L}, \mathbf{x} \rightarrow \mathbf{x}/\mathcal{L}, \mathbf{E} \rightarrow \mathcal{L}\mathbf{E}, \mu \rightarrow \mathcal{L}\mu, \quad (2)$$

the Boltzmann equation in the electrostatic limit, Eq. (1), preserves the solution of the distribution function  $f_e$  and  $f_{j \neq e}$ . This can be easily seen by multiplying  $\mathcal{L}$  and reformulating the Boltzmann equation. The scaling of the collisional rate  $\mathcal{L}\mu$  in Eq. (2) can be realized via scaling the Coulomb Logarithm  $\mathcal{L}\ln\Lambda$  in the plasma simulations, so relative strengths of different collisional processes are preserved. By downsampling the system size with the same factor while holding the plasma speed unchanged, the ratio of the collisional mean free path and the system size or the Knudsen number is unchanged. In cases where the Knudsen number is the critical dimensionless parameter to set the transport physics, for example, in the TQ problem<sup>16</sup>, one can intuitively anticipate the transport physics will be fully captured in the downscaled simulations.

Since the distribution function and particle velocity are both invariant, the moments of the distribution function are invariances as well. These include the density, velocity, temperature, and most interestingly, the electron conduction heat flux, the proper closure of which is required in the fluid modelings of plasmas<sup>14,43,44</sup>. In the collisional limit, the Braginskii

equations for nearly Maxwellian plasmas<sup>43</sup> have both the conduction heat flux  $\mathbf{q}$  and stress tensors  $\Pi$  invariant under the transformation of Eq. (2). Similarly, the electron conduction flux  $\mathbf{q}_e$  in the collisionless regime is also an invariance, either in the free-streaming limit<sup>44</sup>,  $q_e \propto n_e T_{e\parallel} v_{th,e}$  with  $v_{th,e}$  the electron thermal speed, or in the convective scaling regime<sup>14</sup>,  $q_e \propto n_e T_{e\parallel} V_{i\parallel}$  with  $V_{i\parallel}$  the ion flow speed.

Another interesting and important property of the similarity enabled by the transformation Eq. (2) of the electrostatic Boltzmann equation (1) is that the collisional processes, except for the collisional rates, are invariant due to the invariances of the distribution functions. As a result, the downscaled simulations can be applied to a variety of collisional plasmas, e.g., the partially ionized plasma where the nonlinear three-body-type collisions are important<sup>42</sup>. Because the scaled-up collisional rates include the ionization and excitation rates, the plasma cooling rates due to both the ionization and the radiation scale up accordingly, while the “ionization cost,” or the energy dissipation per ionization event<sup>42</sup>, is an atomic physics quantity and unscaled. As a result, the plasma energy density change remains the same due to the downscaled time, though the total plasma energy and its change are scaled down with the system size.

In practice, our downscaled simulation only has explicit control over the system size and the collisional mean free paths, both of which rescale with the same factor  $\mathcal{L}$ . The initial particle distribution  $f(\mathbf{v})$  is not modified. The rescaling of time and electric field are the outcome of the downscaled simulation. Since both the particle transit time  $L/v$  and the collisional time are scaled down by the same factor  $\mathcal{L}$ , the dynamical time in the simulation would be scaled down by  $\mathcal{L}$ , if the associated transport physics is set by the Knudsen number alone. The behavior of the electric field is the most intriguing. In the bulk of the plasma simulation domain, the plasma is quasi-neutral, in which the ambipolar electric field is approximated from the electron momentum equation, e.g., by balancing the electric field force with the electron pressure gradient and the thermal force for nearly-equilibrium plasmas<sup>43</sup>

$$e\mathbf{E} \approx -\frac{1}{n_e} \frac{\partial(n_e T_e)}{\partial \mathbf{x}} - 0.71 n_e \nabla_{\parallel} T_e. \quad (3)$$

Since the density and temperature are invariances, this produces the rescaling  $\mathbf{E} \rightarrow \mathcal{L}\mathbf{E}$ , as desired in Eq. (2) for a “perfect” similarity.

The situation in isolated non-neutral regions is quite different. Since both  $n_e$  and  $T_e$  are invariant under the ideal transformation of Eq. (2), the Debye length  $\lambda_D$  is unchanged. As a result, the electric field in the non-neutral region, which has the original physics scaling of  $T_e/\lambda_D$ , is unaffected in our downscaled simulation. This is actually a desired outcome in that non-neutral plasma region, such as the plasma sheath or the double layer structure in a plasma shock, is tiny in space  $\sim \lambda_D$  compared with the system size  $L$ . Such an extreme scale separation  $L \gg \lambda_D$  presents a natural micro-macro decomposition of the physics. Our downscaled simulations now keep the microscopic physics at its original scale, but preserve the macroscopic transport physics through a similarity transformation.

The scale-up of the macroscopic or quasi-neutral electric

field  $\mathbf{E}$  by a large factor of  $\mathcal{L}$ , as required for the similarity between the full-sized system and the downscaled simulation, comes at the expense of a scaled-up charge separation in a quasi-neutral plasma. This can be seen from the Poisson's equation,

$$\nabla \cdot \mathbf{E} = \frac{q_e}{\epsilon_0} \int (f_e - f_i) d\mathbf{v}. \quad (4)$$

We should highlight again that the electric field scaling can not be obtained from the Poisson's equation<sup>37</sup>, but an automatic outcome of the ambipolar transport. Expressed in terms of Debye length, one finds that ambipolar potential variation  $\Delta\Phi$  in the quasi-neutral plasma, which has a gradient length scale of  $L$ , takes the physical scaling,

$$\frac{e\Delta\Phi}{k_B T_e} \sim \frac{L^2}{\lambda_D^2} \frac{\delta n}{n_0}. \quad (5)$$

Here the plasma potential has the physical scaling  $\Delta\Phi \sim T_e$ , so it is an invariant under the transformation of Eq. (2). In a real plasma, the charge separation ( $\delta n = n_i - n_e$  for a hydrogen plasma) is usually tiny to set up the quasi-neutral electric field,

$$\frac{\delta n}{n_0} \sim \frac{e\Delta\Phi}{k_B T_e} \frac{\lambda_D^2}{L^2} \sim \frac{\lambda_D^2}{L^2}, \quad (6)$$

for the smallness of  $\lambda_D/L$ . In a downscaled simulation,  $L$  is shrunk by a factor of  $\mathcal{L}$  so the effective charge separation is artificially enhanced by a factor of  $\mathcal{L}^2$ .

It may be argued that such enhancement of  $\delta n/n_0$  may be desirable in down-scaled PIC simulations. This is because the PIC code employs the so-called macro-particles that usually represent aggregates of real particles to meet the memory and computation efficiency constraints<sup>1</sup>. As such, the minimum amount of numerical charge separation in the PIC simulations is limited as  $(\delta n/n_0)_{\min} \approx 1/N$  with  $N$  being the number of macro-particles in the cell, which must be larger than  $(\delta n/n_0)_{\min}$  in reality. So an enhancement of a physical  $\delta n$  can reduce the inaccuracy induced by the limited amount of numerical macro-particles. This potential saving in the number of macro-particles required by accuracy is in addition to the computational cost reduction by a shrunk simulation domain compared with  $\lambda_D$  and a shortened dynamical time scale or collisional time  $\tau_c$  compared with the inverse of the plasma frequency  $\omega_{pe}^{-1}$ . Using a one-dimensional configuration space as an example, the total simulation savings simply due to this rescaling of space and time would be a factor of  $\mathcal{L}^2$ .

The weakly collisional or nearly collisionless plasmas allow long-living plasma waves in the electrostatic limit, so the plasma wave-particle interactions can involve additional characteristic lengths and time scales associated with a family of waves with distinct frequencies and wavelengths<sup>45</sup>. One immediate consideration of a downscaled simulation for such a plasma is that the wave frequency, including the real frequency  $\omega_r$  and the growth/damping rate  $\gamma$  with  $\omega = \omega_r + i\gamma$ , and wavelength ( $\lambda = 2\pi/k$ ) are not straightforwardly scaled depending on the wave/instability types. Specifically, since the configuration space is scaled but not the velocity space, the instabilities driven by gradients in configuration space like the

Rayleigh-Taylor and resistive drift wave instabilities<sup>46</sup> should be scaled with  $\mathcal{L}\omega$  and  $\mathcal{L}k$  (note that for the Rayleigh-Taylor instability, the effective gravity,  $g$ , should be scaled as  $\mathcal{L}g$ ). Whereas, the velocity space instabilities like beam instabilities<sup>45,47,48</sup> are not scaled since the distribution function and hence the instability drive is an invariance under the transformation of Eq. (2). As a result, the scaled transport and collisional time may affect the wave properties that can in turn alter the plasma dynamics, e.g., a largely enhanced collisional rate can cause a significant increase of the collisional damping rate of the velocity space instabilities<sup>49</sup>. It should be noted that even though the wave frequencies and wavelengths can be scaled for the configuration space instabilities, the plasma-wave interactions still remain uncertain due to the nonlinear saturation of the instabilities. All these effects will be manifested in the downscaled simulations with different  $\mathcal{L}$ , so the subtlety they can potentially bring to the transport physics can be straightforwardly checked in a  $\mathcal{L}$  scan of downscaled simulations.

Lastly, to ensure that the scaled systems are identical to the original one, all initial and boundary conditions must be scaled consistently. While the initial condition can be straightforwardly scaled, e.g.,  $f(\mathbf{x}/\mathcal{L}, \mathbf{v})$  for the distribution functions, the boundary conditions may differ depending on the specific physical problems. Although it is impractical to list all possible boundary conditions for plasma applications, commonly used ones, such as the periodic<sup>50</sup>, absorbing<sup>29</sup>, and various kinds of recycling<sup>16,51</sup> boundary conditions, generally do not require scaling. For example, the absorbing and recycling boundary conditions depend on the particle flux to the simulation boundaries, which is invariant in this similarity. Although the particle numbers through the boundaries are scaled down due to the reduction of the simulation time, their fractions to the total particle numbers are invariant.

As a demonstration of the proposed similarity, we will consider two one-dimensional (1D) plasma problems using VPIC code<sup>52</sup>. These are dynamic plasma TQ<sup>16</sup> and the steady-state plasma sheath in a high-recycling divertor<sup>51</sup>, which are ideal for demonstrating the similarity properties. Particularly, the plasma in the TQ undergoes a dynamic cooling from the collisionless to the collisional regimes and thus different closures of the electron thermal conduction will be included<sup>16</sup>. It also involves a locally propagating non-neutral shock structure in the collisionless stage<sup>14</sup>. In the plasma sheath problem, the separation of the non-neutral Debye sheath and the quasi-neutral presheath is evident and the Bohm criterion applies to a spatially extended transition layer<sup>29</sup>. More importantly, the plasma sheath in a high-recycling divertor includes complex plasma-neutral interactions such as elastic collision, excitation, ionization, and charge-exchange<sup>51</sup>. In addition, both of these examples contain nontrivial plasma recycling boundary conditions with different types. The VPIC code and simulation setups can be found from Refs. 16, 51, and 52, which are summarized in the supplemental materials.

In the plasma TQ problem, the initial 1D nearly-collisionless plasma has a fixed Knudsen number of  $K_n = \lambda_{mfp}/L_x = 98 \gg 1$ . The cooling boundary will turn the plasma temperature down by 100 times so that the plasma is ini-

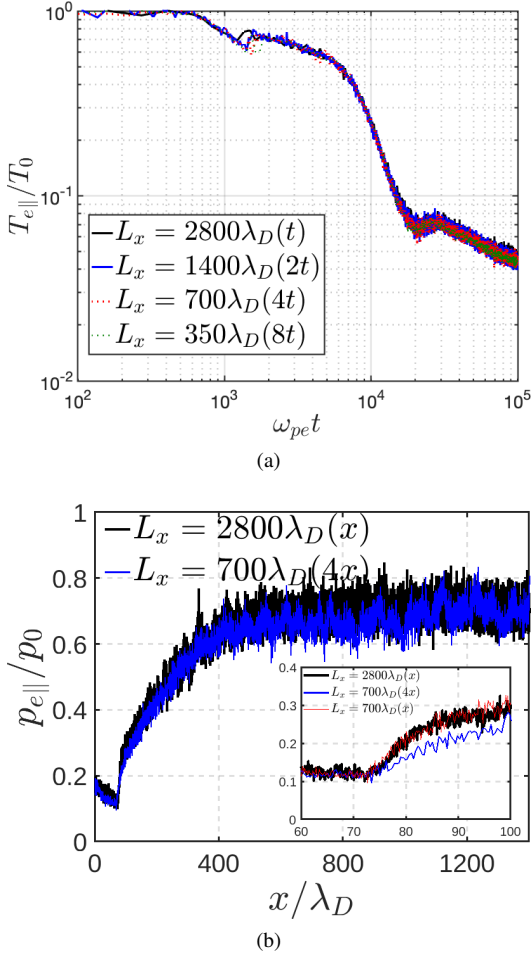


FIG. 1: Results of four scaled TQ simulations with fixing  $K_n = \lambda_{mfp}/L_x = 98$ . (a) Time evolution of the center parallel electron temperature  $T_{e\parallel}$ , in which the time for small  $L_x$  cases ( $L_x < 2800\lambda_D$ ) have been rescaled accordingly. (b) The parallel electron pressure profiles at  $\omega_{pet} = 2000$  for  $L_x = 2800\lambda_D$  (thick black) and at  $\omega_{pet} = 500$  for  $L_x = 700\lambda_D$  (thin blue), where the spatial coordinate for the latter is quadrupled. In the zoom-in figure near the shock front around  $x = 74\lambda_D$ , we also plot  $p_{e\parallel}$  for  $L_x = 700\lambda_D$  case (thinnest red) with the original spatial coordinate (but shifted so that its shock front co-locates with the other two). A reduced ion-to-electron mass ratio of  $m_i = 100m_e$  is employed. The Debye length for the initial hot plasma,  $\lambda_D \propto \sqrt{T_0/n_0}$  is used for normalization.

tially nearly-collisionless but eventually collisional as a result of cooling. The results of four similar simulations with different  $L_x$  are shown in Fig. 1, demonstrating nearly identical plasma TQ processes. Particularly, the time evolution of the center electron temperature in Fig. 1(a) indicates that the electron thermal conduction flux should be an invariance in both the collisionless ( $\omega_{pet} < 2 \times 10^4$ ) and collisional regimes ( $\omega_{pet} > 2 \times 10^4$ ). While the electron pressure  $p_{e\parallel} = n_e T_{e\parallel}$  profiles in Fig. 1(b) provide another straightforward evidence of the similarity. As aforementioned,  $p_{e\parallel}$  also manifests the

electric field under the ambipolar transport constraint in the nearly-collisionless plasma since its gradient balances with the electric force<sup>14</sup>, i.e.,  $E_x \propto \partial p_{e\parallel}/\partial x$ . In fact, it is more practical to use  $p_{e\parallel}$  rather than  $E_x$  itself to illustrate the scaling laws of the electric field since  $E_x$  suffers Langmuir perturbations as shown in Fig. 1(b) that is not invariant. We see that  $p_{e\parallel}$  in the bulk plasma is nearly the same, reminiscent of an enhancement of  $E_x$  in the cases with small  $L_x$ . More importantly, the zoom-in plot near the shock front around  $x = 74\lambda_D$  shows that the shock front structure and hence the associated electric field is not scaled by comparing the  $p_{e\parallel}$  profiles in the original coordinates (the thick black and thin red curves).

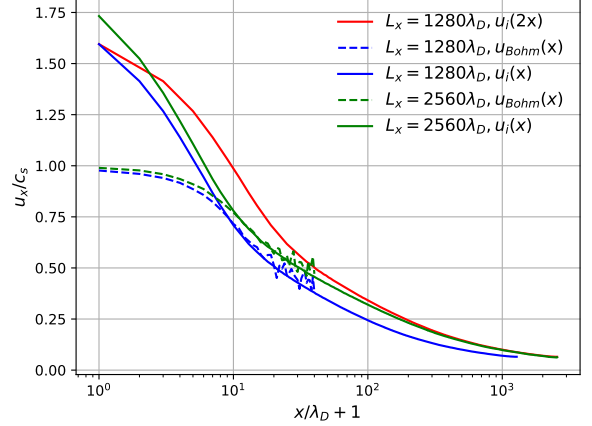


FIG. 2: Ion exit flow and the Bohm speed in Eq. (7), normalized by local  $c_s = \sqrt{(T_{ex} + 3T_{ix})/m_i}$ , in two scaled sheath simulations. For the  $L_x = 1280\lambda_D$  case, both the original and rescaled results in terms of the spatial coordinates are included. Here  $\lambda_D$  is for a plasma with  $T_e = 10\text{eV}$  and  $n_e = 5 \times 10^{19}\text{m}^{-3}$ .

In the plasma sheath simulations, a power input,  $Q_{in}$ , at the right boundary is utilized to supply the power for the plasma cooling and neutral ionization in the whole domain. The energy input should be scaled with the total particles and hence the system domain, but not the power input due to the scaled time. Thus, this power input through a unit surface area from the boundary is different from the power density that should be scaled up just as the radiative cooling rate. Here  $Q_{in} = 10\text{MW/m}^2$  is used for an averaged plasma density of  $\bar{n} = \int_0^{L_x} (n_i + n_n) dx / L_x = 10^{20}\text{m}^{-3}$  with  $n_i$  and  $n_n$  being the ion and neutral density, respectively. In such a problem, a complex Bohm criterion that gives the lower bound of the ion exit flow speed of  $u_{Bohm}$  applies to a wide transition layer by considering all the transport physics<sup>51</sup>

$$u_{ix} \geq u_{Bohm} \equiv \sqrt{(3T_{ix} + \beta_{Bohm} T_{ex})/m_i}, \quad (7)$$

where  $\beta_{Bohm}$

$$\beta_{Bohm} \equiv -\frac{3 \left( \frac{\partial q_n^i / \partial \phi}{en_i u_{ix}} - 1 + \frac{J_{ixx}}{e\Gamma_i E} - \frac{I_{ix}}{en_i E} \right)}{\frac{\partial q_n^e / \partial \phi}{en_e u_{ex}} + 1 + \frac{J_{exx}}{en_e u_{ex} E} - \frac{I_{ex}}{en_e E}}. \quad (8)$$

Here  $q_n$  is the thermal conduction flux of  $x$ -degree of freedom in the  $x$  direction, and  $I_x$  and  $J_{xx}$  is, respectively, the sum of momentum and energy change in the  $x$  direction due to all collisions. All these terms can be evaluated locally in VPIC simulations, where time-averaged plasma parameters over a long time period in the steady state are utilized to suppress the PIC noises in contrast to the post-process denoising approach<sup>53</sup>. Two simulations with different  $L_x$  and corresponding mean free paths are conducted, with the steady-state ion exit flow and Bohm speed  $u_{Bohm}$  shown in Fig. 2. It shows that the plasma behaviors in the bulk region  $x \gtrsim 100\lambda_D$  are nearly identical by comparing the rescaled results (the red and the green). While the plasma sheath is almost not scaled (e.g., see the blue and the green), the nominal entrance of which is denoted by the separation of  $u_i$  from  $u_{Bohm}$ .

In conclusion, a simple but powerful similarity was discussed for kinetic simulations of electrostatic plasmas, in which the characteristic lengths including the system size and mean free paths are reduced in contrast to the small invariant Debye length. The similarity properties and its applicability have been discussed. The utility of this similarity has been showcased by VPIC simulations of the dynamic TQ and the steady-state plasma (pre)sheath in a high recycling divertor.

**Acknowledgment** We thank the U.S. Department of Energy Office of Fusion Energy Sciences through the Base Fusion Theory Program at Los Alamos National Laboratory (LANL) under contract No. 89233218CNA000001. This research used resources of the National Energy Research Scientific Computing Center, a DOE Office of Science User Facility supported by the Office of Science of the U.S. Department of Energy under Contract No. DE-AC02-05CH11231 using NERSC award FES-ERCAP0032298 and LANL Institutional Computing Program, which is supported by the U.S. Department of Energy National Nuclear Security Administration under Contract No. 89233218CNA000001.

- <sup>1</sup>C. K. Birdsall and A. B. Langdon, *Plasma physics via computer simulation* (CRC press, 2018).
- <sup>2</sup>T. Tajima, *Computational plasma physics: with applications to fusion and astrophysics* (CRC press, 2018).
- <sup>3</sup>J. P. Verboncoeur, “Particle simulation of plasmas: review and advances,” *Plasma Physics and Controlled Fusion* **47**, A231 (2005).
- <sup>4</sup>C.-Z. Cheng and G. Knorr, “The integration of the vlasov equation in configuration space,” *Journal of Computational Physics* **22**, 330–351 (1976).
- <sup>5</sup>F. Filbet and E. Sonnendrücker, “Comparison of eulerian vlasov solvers,” *Computer Physics Communications* **150**, 247–266 (2003).
- <sup>6</sup>Y. Cheng, I. M. Gamba, F. Li, and P. J. Morrison, “Discontinuous galerkin methods for the vlasov–maxwell equations,” *SIAM Journal on Numerical Analysis* **52**, 1017–1049 (2014).
- <sup>7</sup>E. Doyle, W. Houlberg, Y. Kamada, V. Mukhovatov, T. Osborne, A. Polovoi, G. Bateman, J. Connor, J. C. (retired), T. Fujita, X. Garbet, T. Hahm, L. Horton, A. Hubbard, F. Imbeaux, F. Jenko, J. Kinsey, Y. Kishimoto, J. Li, T. Luce, Y. Martin, M. Ossipenko, V. Parail, A. Peeters, T. Rhodes, J. Rice, C. Roach, V. Rozhansky, F. Ryter, G. Saibene, R. Sartori, A. Sips, J. Snipes, M. Sugihara, E. Synakowski, H. Takenaga, T. Takizuka, K. Thomsen, M. Wade, H. Wilson, I. T. P. T. Group, I. C. Database, M. Group, I. Pedestal, and E. T. Group, “Chapter 2: Plasma confinement and transport,” *Nuclear Fusion* **47**, S18–S127 (2007).
- <sup>8</sup>P. Rodriguez-Fernandez, A. Creely, M. Greenwald, D. Brunner, S. Ballinger, C. Chrobak, D. Garnier, R. Granetz, Z. Hartwig, N. Howard, J. Hughes, J. Irby, V. Izzo, A. Kuang, Y. Lin, E. Marmar, R. Mumgaard, C. Rea, M. Reinke, V. Riccardo, J. Rice, S. Scott, B. Sorbom, J. Stillerman, R. Sweeney, R. Tinguely, D. Whyte, J. Wright, and D. Yuryev, “Overview of the SPARC physics basis towards the exploration of burning-plasma regimes in high-field, compact tokamaks,” *Nuclear Fusion* **62**, 042003 (2022).
- <sup>9</sup>N. R. Council, *Plasma Science: Advancing Knowledge in the National Interest* (The National Academies Press, Washington, DC, 2007).
- <sup>10</sup>G. Parks, “Magnetosphere,” in *Encyclopedia of Atmospheric Sciences (Second Edition)*, edited by G. R. North, J. Pyle, and F. Zhang (Academic Press, Oxford, 2015) second edition ed., pp. 309–315.
- <sup>11</sup>I. Zhuravleva, E. Churazov, A. A. Schekochihin, S. W. Allen, P. Arévalo, A. C. Fabian, W. R. Forman, J. S. Sanders, A. Simionescu, R. Sunyaev, A. Vikhlinin, and N. Werner, “Turbulent heating in galaxy clusters brightest in x-rays,” *Nature* **515**, 85–87 (2014).
- <sup>12</sup>Z. Guo and X.-Z. Tang, “Ambipolar transport via trapped-electron whistler instability along open magnetic field lines,” *Physical Review Letters* **109**, 135005 (2012).
- <sup>13</sup>X.-Z. Tang and Z. Guo, “Kinetic model for the collisionless sheath of a collisional plasma,” *Physics of Plasmas* **23**, 083503 (2016).
- <sup>14</sup>Y. Zhang, J. Li, and X.-Z. Tang, “Cooling flow regime of a plasma thermal quench,” *Europhysics Letters* **141**, 54002 (2023).
- <sup>15</sup>Y. Zhang, J. Li, and X.-Z. Tang, “Electron heat flux and propagating fronts in plasma thermal quench via ambipolar transport,” *Physics of Plasmas* **30**, 092301 (2023).
- <sup>16</sup>J. Li, Y. Zhang, and X.-Z. Tang, “Staged cooling of a fusion-grade plasma in a tokamak thermal quench,” *Nuclear Fusion* **63**, 066030 (2023).
- <sup>17</sup>A. C. Fabian, “Cooling flows in clusters of galaxies,” *Annual Review of Astronomy and Astrophysics* **32**, 277–318 (1994), <https://doi.org/10.1146/annurev.aa.32.090194.001425>.
- <sup>18</sup>J. Peterson and A. Fabian, “X-ray spectroscopy of cooling clusters,” *Physics Reports* **427**, 1–39 (2006).
- <sup>19</sup>F. F. Chen, *Introduction to plasma physics* (Springer Science & Business Media, 2012).
- <sup>20</sup>L. Tonks and I. Langmuir, “A general theory of the plasma of an arc,” *Phys. Rev.* **34**, 876–922 (1929).
- <sup>21</sup>I. Langmuir, “The interaction of electron and positive ion space charges in cathode sheaths,” *Phys. Rev.* **33**, 954–989 (1929).
- <sup>22</sup>M. A. Lieberman and A. J. Lichtenberg, *Principles of Plasma Discharges and Materials Processing*, 2nd ed. (Wiley-Interscience, 2005).
- <sup>23</sup>P. C. Stangeby, *The Plasma Boundary of Magnetic Fusion Devices* (Taylor & Francis, 2000).
- <sup>24</sup>R. Taylor, D. Baker, and H. Ikezi, “Observation of collisionless electrostatic shocks,” *Physical Review Letters* **24**, 206 (1970).
- <sup>25</sup>L. Romagnani, S. Bulanov, M. Borghesi, P. Audebert, J. Gauthier, K. Löwenbrück, A. Mackinnon, P. Patel, G. Pretzler, T. Toncian, *et al.*, “Observation of collisionless shocks in laser-plasma experiments,” *Physical review letters* **101**, 025004 (2008).
- <sup>26</sup>D. Forslund and C. Shonk, “Formation and structure of electrostatic collisionless shocks,” *Physical Review Letters* **25**, 1699 (1970).
- <sup>27</sup>G. Sarri, M. E. Dieckmann, I. Kourakis, and M. Borghesi, “Shock creation and particle acceleration driven by plasma expansion into a rarefied medium,” *Physics of Plasmas* **17**, 082305 (2010).
- <sup>28</sup>S. Moiseev and R. Sagdeev, “Collisionless shock waves in a plasma in a weak magnetic field,” *Journal of Nuclear Energy. Part C, Plasma Physics, Accelerators, Thermonuclear Research* **5**, 43 (1963).
- <sup>29</sup>Y. Li, B. Srinivasan, Y. Zhang, and X.-Z. Tang, “Bohm criterion of plasma sheaths away from asymptotic limits,” *Phys. Rev. Lett.* **128**, 085002 (2022).
- <sup>30</sup>Y. Li, B. Srinivasan, Y. Zhang, and X.-Z. Tang, “Transport physics dependence of bohm speed in presheath–sheath transition,” *Physics of Plasmas* **29**, 113509 (2022), <https://doi.org/10.1063/5.0110379>.
- <sup>31</sup>T. Takizuka, “Kinetic effects in edge plasma: kinetic modeling for edge plasma and detached divertor,” *Plasma Physics and Controlled Fusion* **59**, 034008 (2017).
- <sup>32</sup>D. Ryutov and B. Remington, “A “perfect” hydrodynamic similarity and effect of the reynolds number on the global scale motion,” *Physics of Plasmas* **10**, 2629–2632 (2003).
- <sup>33</sup>Y. Fu, H. Wang, B. Zheng, P. Zhang, Q. H. Fan, X. Wang, and J. P. Verboncoeur, “Generalizing similarity laws for radio-frequency discharge plasmas across nonlinear transition regimes,” *Physical Review Applied* **16**, 054016 (2021).
- <sup>34</sup>Z. Duan, Z. Zhao, Z. Wang, and Y. Fu, “Evaluation of the similarity properties of double-headed streamer propagation,” *IEEE Transactions on Dis-*

electronics and Electrical Insulation (2024).

<sup>35</sup>B. Zheng, Y. Fu, K. Wang, H. Wang, L. Chen, T. Schuelke, and Q. H. Fan, “Scale-invariant breathing oscillations and transition of the electron energization mechanism in magnetized discharges,” *Applied Physics Letters* **124** (2024).

<sup>36</sup>D. Yang, J. P. Verboncoeur, and Y. Fu, “Demonstration of similarity laws and scaling networks for radio-frequency plasmas,” *Physical Review Letters* **134**, 045301 (2025).

<sup>37</sup>Y. Fu, H. Wang, and X. Wang, “Similarity theory and scaling laws for low-temperature plasma discharges: A comprehensive review,” *Reviews of Modern Plasma Physics* **7**, 10 (2023).

<sup>38</sup>E. Buckingham, “On physically similar systems; illustrations of the use of dimensional equations,” *Physical review* **4**, 345 (1914).

<sup>39</sup>D. Ryutov, “Scaling laws for dynamical plasma phenomena,” *Physics of Plasmas* **25** (2018).

<sup>40</sup>M. Murakami and S. Iida, “Scaling laws for hydrodynamically similar implosions with heat conduction,” *Physics of Plasmas* **9**, 2745–2753 (2002).

<sup>41</sup>E. Falize, C. Michaut, and S. Bouquet, “Similarity properties and scaling laws of radiation hydrodynamic flows in laboratory astrophysics,” *The Astrophysical Journal* **730**, 96 (2011).

<sup>42</sup>S. Krasheninnikov, A. Smolyakov, and A. Kukushkin, *On the edge of magnetic fusion devices* (Springer, 2020).

<sup>43</sup>S. I. Braginskii, *Reviews of Plasma Physics*, ed. M. A. Leontovich, Vol. I, pp. 205–311 (Consultants Bureau, New York, 1965).

<sup>44</sup>A. R. Bell, “Non-spitzer heat flow in a steadily ablating laser-produced plasma,” *The Physics of Fluids* **28**, 2007–2014 (1985), <https://aip.scitation.org/doi/10.1063/1.865378>.

<sup>45</sup>T. H. Stix, *Waves in plasmas* (Springer Science & Business Media, 1992).

<sup>46</sup>Y. Zhang, S. Krasheninnikov, and A. Smolyakov, “Different responses of the rayleigh–taylor type and resistive drift wave instabilities to the velocity shear,” *Physics of Plasmas* **27**, 020701 (2020).

<sup>47</sup>J. M. Dawson, “Plasma oscillations of a large number of electron beams,” *Physical Review* **118**, 381 (1960).

<sup>48</sup>O. Buneman, “Excitation of field aligned sound waves by electron streams,” *Physical Review Letters* **10**, 285 (1963).

<sup>49</sup>S. Auerbach, “Collisional damping of langmuir waves in the collisionless limit,” Tech. Rep. (Princeton Plasma Physics Lab.(PPPL), Princeton, NJ (United States), 1977).

<sup>50</sup>Y. Zhang and X.-Z. Tang, “On the collisional damping of plasma velocity space instabilities,” *Physics of Plasmas* **30**, 030701 (2023).

<sup>51</sup>Y. Li, B. Srinivasan, Y. Zhang, and X.-Z. Tang, “The plasma–sheath transition and bohm criterion in a high recycling divertor,” *Physics of Plasmas* **30**, 063505 (2023).

<sup>52</sup>K. J. Bowers, B. Albright, L. Yin, B. Bergen, and T. Kwan, “Ultrahigh performance three-dimensional electromagnetic relativistic kinetic plasma simulation,” *Physics of Plasmas* **15**, 055703 (2008).

<sup>53</sup>M. J. Picklo, Q. Tang, Y. Zhang, J. K. Ryan, and X.-Z. Tang, “Denoising particle-in-cell data via smoothness-increasing accuracy-conserving filters with application to bohm speed computation,” *Journal of Computational Physics* **502**, 112790 (2024).

<sup>54</sup>K. Nanbu, “Probability theory of electron-molecule, ion-molecule, molecule-molecule, and coulomb collisions for particle modeling of materials processing plasmas and cases,” *IEEE Transactions on plasma science* **28**, 971–990 (2000).

<sup>55</sup>P. Helander and D. J. Sigmar, *Collisional transport in magnetized plasmas*, Vol. 4 (Cambridge university press, 2005).

<sup>56</sup>H. Wang, D. Yang, B. Zheng, and Y. Fu, “Similarity rules for inductive radio frequency plasmas with thermohydrodynamic coupling effects,” *Journal of Applied Physics* **134** (2023).

<sup>57</sup>Y. Zhang, J. Li, and X.-Z. Tang, “Collisionless cooling of perpendicular electron temperature in the thermal quench of a magnetized plasma,” *Scientific Reports* **14**, 23448 (2024).

<sup>58</sup>C. F. Kennel and H. Petschek, “Limit on stably trapped particle fluxes,” *Journal of Geophysical Research* **71**, 1–28 (1966).

## SUPPLEMENTAL MATERIAL TO ‘SIMILARITY FOR DOWNSCALED KINETIC SIMULATIONS OF ELECTROSTATIC PLASMAS: RECONCILING THE LARGE SYSTEM SIZE WITH SMALL DEBYE LENGTH’

### I. VPIC CODE, SIMULATION SETUPS AND DIAGNOSTICS

VPIC<sup>52</sup> is a general purpose particle-in-cell simulation code for modeling kinetic plasmas in one, two, or three spatial dimensions. It employs a second-order, explicit, leapfrog algorithm to update charged particle positions and velocities in order to solve the relativistic kinetic equation for each species in the plasma, along with a full Maxwell description for the electric and magnetic fields evolved via a second-order finite-difference-time-domain (FDTD) solve. A Monte Carlo collision (MCC) module with null collision method<sup>54</sup> is developed in VPIC to handle the collisions<sup>51</sup>. In such module, a constant Coulomb Logarithm is provided by the user to quantify the collisional rates.

In the plasma TQ problem<sup>16</sup>, an initial 1D uniform plasma with temperature  $T_0 = 10\text{eV}$  and density  $n_0 = 10^{20}\text{m}^{-3}$  is bounded by the thermobath boundaries at the two ends, which recycle plasma particles but clamp the temperature of the recycled plasma particles to  $T_w = 0.01T_0$ . The cell size and number of macro-particles per cell are the same in different simulations, except for the smallest  $L_x = 350\lambda_D$  case where doubled macro-particles per cell have been used to reduce the simulation noise, which reaffirms the advantage of system size reduction. The initial Knudsen number is fixed as  $K_n = \lambda_{mfp}/L_x = 98 \gg 1$  so that the plasma is initially nearly collisionless but eventually collisional as a result of cooling towards the temperature  $T_w$ .

For simulating the plasma sheath in a high-recycling divertor, a “closed box” setup is employed following Ref. 51: a recycling tungsten wall is implemented at the left boundary of the simulation domain with a unit total particle recycling coefficient (including the reflected particles associated with a comprehensive wall energy recycling coefficient and desorbed particles with wall temperature); while a power input at the right boundary is utilized to supply the power for the plasma cooling and neutral ionization in the whole domain. Interested readers are recommended to read Ref. 51 for detailed implementation.

In the simulations, the plasma density, parallel flow, parallel temperature and thermal conduction heat flux of the parallel degrees are calculated following the statistic physics from the particle distribution function  $f$ ,

$$n = \int f d^3v, \quad (9)$$

$$nV_x = \int v_x f d^3v, \quad (10)$$

$$nT_x = m \int (v_x - V_x)^2 f d^3v, \quad (11)$$

$$q_n = m \int (v_x - V_x)^3 f d^3v. \quad (12)$$

Thus, the “temperature” cannot be used to describe the

“slope” of the total electron distribution but measures the kinetic energy spread around a mean flow for particles.

## II. BACKGROUND MAGNETIC FIELD AND ELECTROMAGNETIC EFFECTS

The downscaled electrostatic kinetic simulations can offer remarkable property of near-perfect similarity in multi-dimensional unmagnetized plasmas or in 1D magnetized plasmas along the magnetic field, as shown in the main body of the paper. In the electrostatic simulations of multi-dimensional magnetized plasmas, the PIC approach may need to be modified though the similarity still holds. To see this formally, we recall that the Boltzmann equation with magnetic field has the form

$$\frac{\partial f_e}{\partial t} + \mathbf{v} \cdot \frac{\partial f_e}{\partial \mathbf{x}} + \frac{q_e}{m_e} (\mathbf{E} + \mathbf{v} \times \mathbf{B}) \cdot \frac{\partial f_e}{\partial \mathbf{v}} = \sum_j C_{ej}(f_e, f_j, \mathbf{v}_{ej}, \sigma_{ej}), \quad (13)$$

where  $\mathbf{B}$  is a constant in the electrostatic limit but can change in time to account for the electromagnetic effects. For  $f$  to remain unchanged under the transformation, the magnetic field must follow the transformation or rescaling of  $\mathbf{B} \rightarrow \mathcal{L}\mathbf{B}$ . With a background magnetic field, this will alter several plasma properties including the plasma beta,  $\beta \propto n_e T_e / B^2 \propto 1/\mathcal{L}^2$ , the Alfvén speed,  $V_A \propto B/\sqrt{n} \propto \mathcal{L}$ , and the particle gyro-radii  $\rho_{e,i} \propto v_{ih,e,i}/\omega_{ce,i} \propto 1/\mathcal{L}$ , etc.

In the electrostatic limit, these modified quantities by  $\mathbf{B}$  may not affect the transport physics. For example, the particle drift velocities are not scaled but the banana orbit width is reduced by a factor of  $\mathcal{L}$  in tokamaks so that the neoclassical transport is invariant<sup>55</sup>.

However, there are two potential issues in the multi-dimensional magnetized plasmas even in the electrostatic limit, which can appear in the electromagnetic plasmas as well though the electromagnetic effects are more complicated. The first issue is that the multi-dimensionality of the plasma may induce new instabilities, like the resistive drift wave instabilities in tokamaks<sup>46</sup>, that introduce new time and length scales into the system. These instabilities may depend on the background magnetic field or not. As discussed in the main body of the paper, the instabilities and associated waves themselves already challenge the applicability of the proposed similarity, while the scaling of  $\mathcal{L}\mathbf{B}$  simply make the situation more complicated. The second issue arises when the plasma has a large electron gyrofrequency,  $\omega_{ce} \gtrsim \omega_{pe}$ . In such case, the simulation time step,  $\Delta t$ , in the scaled simulations with much enhanced  $\mathbf{B}$  and hence  $\omega_{ce}$  is limited by the requirement of resolving the gyro-motion ( $\omega_{ce}\Delta t < 1$ ) rather than the CFL constraint. Thus, the saving factor is reduced, e.g., from  $\mathcal{L}$  to  $\mathcal{L}$  in 1D case. One possible solution to this issue can be applying the guiding-center motion for electrons to avoid the requirement of resolving  $\omega_{ce}$ <sup>31</sup>.

In the electromagnetic limit, the application of this scaling is more subtle. For cases where the physics is not de-

pendent on the aforementioned scaled variables related to  $\mathbf{B}$ , the scaling of  $\mathcal{L}\mathbf{B}$  still works, as in Ref.<sup>56</sup>. However, for the plasma transport that indeed depend on the plasma beta, Alfvén speed, etc., the downscaled kinetic simulations can no longer capture the correct physics. For such case, one can alternatively decide not to scale  $\mathbf{B}$  so the plasma beta stays the same in the downscaled simulations. Whether the relevant physics is properly captured in such simulations requires case-by-case examinations. An illustrative example we have encountered is again in the plasma thermal quench problem. The issue is that in the electrostatic limit, plasma cooling as a result of rapid parallel transport to the boundary, as envisioned for a globally stochastic magnetic field, brings down the  $T_{e\parallel}$  rapidly but not the  $T_{e\perp}$  (e.g., see Fig. 3 in the supplemental materials). An intriguing question is whether there are collisionless cooling mechanisms that can bring down  $T_{e\perp}$  at the rate by which  $T_{e\parallel}$  is cooled by the parallel transport<sup>57</sup>. One plausible candidate is the velocity-space whistler wave instability, previously known from Ref.<sup>12</sup>, for a truncated electron distribution, which is an electromagnetic wave instability. Although the strength of the magnetic field does not affect the formation of the truncated electron distribution and hence  $T_{e\parallel}$  cooling, which is due to tail electron loss through parallel transport, it does impact the dispersion of the unstable whistler modes,<sup>58</sup> so the background magnetic field should not be scaled. For such a velocity-space instability, rescaling the system with the exception of the background magnetic field thus has no effect on the dispersion and growth rate of the modes, as long as the wavelength is short compared with the downscaled system size. Again, the benefit of such downscaled electromagnetic simulations without B-rescaling is particularly great for this problem since  $\omega_{ce} \gtrsim \omega_{pe}$ . As a result, the perturbed quantities including the electromagnetic fields and current are invariances, although one needs to care about the enhanced collisional damping effect in the downscaled system<sup>50,57</sup>.

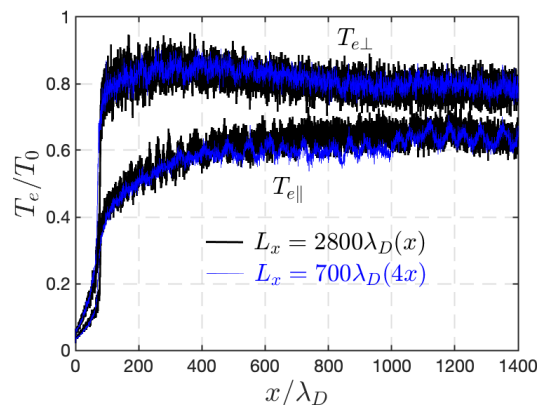


FIG. 3: The parallel and perpendicular electron temperature in the thermal quench simulations, corresponding to Fig. 1b in the main body of the paper.